Electrocatalysis

International Edition: DOI: 10.1002/anie.201408998
German Edition: DOI: 10.1002/ange.201408998

$SrNb_{0.1}Co_{0.7}Fe_{0.2}O_{3-\delta}$ Perovskite as a Next-Generation Electrocatalyst for Oxygen Evolution in Alkaline Solution**

*Yinlong Zhu, Wei Zhou, Zhi-Gang Chen, Yubo Chen, Chao Su, Moses O. Tadé, and Zongping Shao**

Abstract: *The perovskite $SrNb_{0.1}Co_{0.7}Fe_{0.2}O_{3-\delta}$ (SNCF) is a promising OER electrocatalyst for the oxygen evolution reaction (OER), with remarkable activity and stability in alkaline solutions. This catalyst exhibits a higher intrinsic OER activity, a smaller Tafel slope and better stability than the state-of-the-art precious-metal IrO_2 catalyst and the well-known BSCF perovskite. The mass activity and stability are further improved by ball milling. Several factors including the optimized e_g orbital filling, good ionic and charge transfer abilities, as well as high OH^- adsorption and O_2 desorption capabilities possibly contribute to the excellent OER activity.*

As global energy demand is rapidly increasing, the discovery of cost-effective, highly active catalysts for energy conversion and storage is of prime importance in the societal pursuit of sustainable energy.[1] Among potential electrochemical processes, the oxygen evolution reaction (OER) during water oxidation is the key step for renewable-energy technologies, such as water splitting, rechargeable metal–air batteries, and regenerative fuel cells.[2] However, the kinetics of OER ($2H_2O \leftrightarrow 4H^+ + O_2 + 4e^-$ in acidic media or $4OH^- \leftrightarrow 2H_2O + O_2 + 4e^-$ in alkaline media) are sluggish and often require a considerable overpotential relative to thermodynamic potential of the reaction (1.23 V vs reversible hydrogen electrode, RHE, at standard temperature and pressure) to reach a desirable current density, such as $10\,mA\,cm^{-2}$ (on a basis of 10% solar-to-fuel conversion efficiency).[3] Thus, the development of efficient electrocatalysts with low overpotential and good long-term stability in OER catalysis is constantly being pursued. Currently, IrO_2 and RuO_2 have been identified as the most active catalysts for the OER, but the scarcity and high cost of each limit their wide application.[4] Accordingly, extensive research is urgently needed to develop alternative OER electrocatalysts that are inexpensive, sufficiently active, and stable upon prolonged exposure to oxidizing conditions in alkaline solutions. Over the years, a great number of alternative OER catalysts based on abundant 3d transition metals have been studied, including metal oxides (hydroxides),[5] chalcogenides,[6] phosphates,[3a,7] molecular compounds,[8] and advanced metal oxides/carbon composite catalysts.[9]

ABO_3-type oxides known as perovskites, where A is commonly a rare-earth or alkaline earth element and B is commonly a transition metal, are widely used in solid oxide fuel cells (SOFCs) and oxygen permeation membranes.[10] Perovskite oxides have lately been of particular interest for renewable-energy technologies owing to their reported high specific catalytic activity ($mA\,cm^{-2}_{oxide}$) toward the OER in alkaline conditions.[11] Suntivich et al. reported a descriptor to rational design perovskite (ABO_3) electrocatalysts with high OER activity. They found that a near-unity occupancy of the e_g orbital of the first-row transition metal in the perovskite oxides can enhance the intrinsic activity for the OER in alkaline solution.[11a] Based on this descriptor, $Ba_{0.5}Sr_{0.5}Co_{0.8}Fe_{0.2}O_{3-\delta}$ (BSCF) and $SrCo_{0.8}Fe_{0.2}O_{3-\delta}$ (SCF) perovskites have been developed as highly active catalysts, with intrinsic activity significantly surpassing that of the state-of-the-art precious-metal IrO_2.[11a,12] However, BSCF and SCF materials readily undergo changes in their local structure, switching from corner-sharing to edge-sharing octahedral with concomitant formation of an amorphous phase under OER conditions.[12] As a consequence, substantial progress is still needed to develop perovskite-type OER catalysts with improved activity and stability.

Herein, we report a novel perovskite $SrNb_{0.1}Co_{0.7}Fe_{0.2}O_{3-\delta}$ (SNCF) as a highly active catalyst for the OER in alkaline solution. The SNCF perovskite showed higher intrinsic OER activity than IrO_2 catalyst and BSCF perovskite. This enhanced OER activity may be attributed to the optimized e_g orbital filling, good ionic and charge transfer abilities, as well as high OH^- adsorption and O_2 desorption capabilities. The SNCF perovskite also exhibited excellent durability under harsh OER cycling conditions. Furthermore, the mass activity and stability of SNCF can be further enhanced by ball milling (the ball-milled SNCF sample is noted as SNCF-BM). These results strongly suggest the potential for an efficient,

[*] Y. L. Zhu, Prof. W. Zhou, Y. B. Chen, Prof. Z. P. Shao
State Key Laboratory of Materials-Oriented Chemical Engineering
College of Chemistry & Chemical Engineering, Nanjing Tech University
No. 5 Xin Mofan Road, Nanjing 210009 (P.R. China)
E-mail: shaozp@njtech.edu.cn
Dr. Z. G. Chen
School of Materials Engineering, University of Queensland
Brisbane, Queensland 4072 (Australia)
Dr. C. Su, Prof. M. O. Tadé, Prof. Z. P. Shao
Department of Chemical Engineering, Curtin University
Perth, Western Australia 6845 (Australia)

[**] This work was supported by the Key Projects in Nature Science Foundation of Jiangsu Province under contract No. BK2011030, by the National Science Foundation for Distinguished Young Scholars of China under contract No. 51025209, by the "National Nature Science Foundation of China" under contract No. 21103089, and by the Priority Academic Program Development of Jiangsu Higher Education Institutions (PAPD).

Supporting information for this article is available on the WWW under http://dx.doi.org/10.1002/anie.201408998.

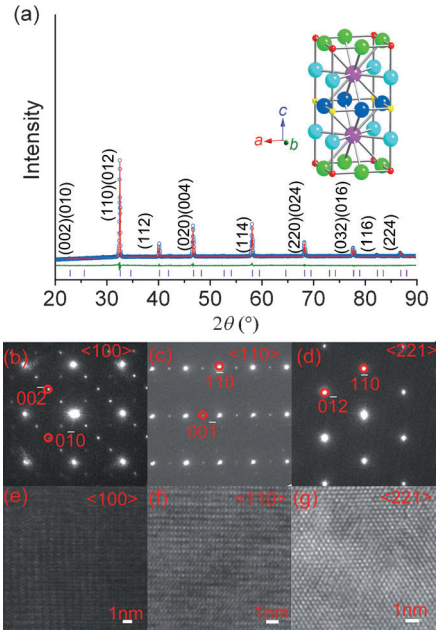

Figure 1. a) Refined X-ray diffraction (XRD) profiles of the SNCF sample. Observed (blue circles), calculated (red solid line), differences (green line, bottom), and calculated Bragg positions (vertical purple bars) for each phase are presented. Inset: the tetragonal SNCF crystal structure (Sr purple, Co red/yellow, O green/pale and dark blue. The position of Fe and Nb is the same as Co. b) SAED patterns (b–d) and the corresponding HRTEM images (e–g) of the ⟨100⟩, ⟨110⟩, ⟨221⟩ zone axes for SNCF.

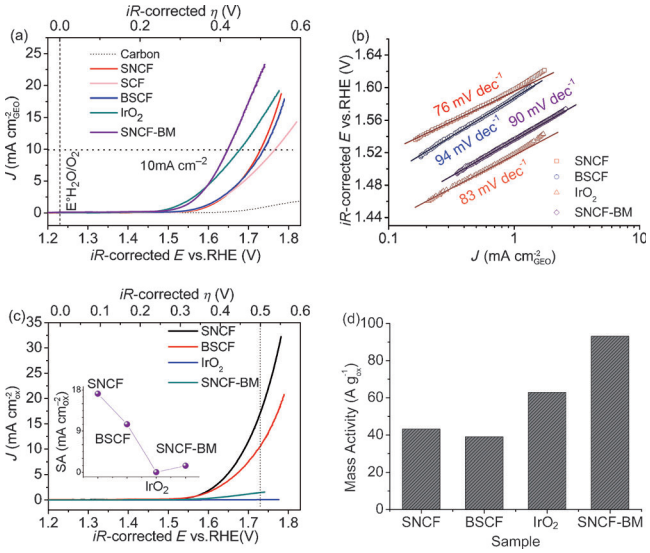

Figure 2. a) Linear sweeping voltammograms (LSVs) for the OER on rotating disk electrodes comprised of the SNCF, SCF, BSCF, IrO_2, and SNCF-BM catalysts in O_2-saturated 0.1 M KOH solution at 1600 rpm. The background OER activity of a thin-film Nafion-bonded carbon thin-film electrode is shown for reference. b) Tafel plots of the SNCF, BSCF, IrO_2 and SNCF-BM catalysts. c) OER specific activity (SA) of the SNCF, BSCF, IrO_2, and SNCF-BM catalysts as a function of potential. Inset: specific activity of the SNCF, BSCF, IrO_2, and SNCF-BM catalysts at an overpotential of $\eta = 0.5$ V. d) Mass activity (MA) based on the oxide weight of the SNCF, BSCF, IrO_2, and SNCF-BM catalysts at an overpotential of $\eta = 0.5$ V.

robust, and economic OER electrocatalyst based on SNCF perovskite oxide.

The phase structure of SNCF was first analyzed by room-temperature X-ray diffraction (RT-XRD) with the typical pattern presented in Figure 1 a. Rietveld refinement revealed the SNCF to possess a tetragonal structure with lattice parameters of $a = 3.8808$ Å and $c = 7.7679$ Å and a space group of *P*4/*mmm*. The reliability of the Rietveld refinement is $R_p = 1.29\,\%$, $R_{wp} = 2.24\,\%$, and $\chi^2 = 1.74$, which is satisfactory with respect to goodness of fit. The inset in Figure 1 a depicts the crystal structure of the tetragonal SNCF perovskite. The tetragonal phase structure of SNCF was further confirmed by three key selected-area electron-diffraction (SAED) patterns along the three ⟨100⟩, ⟨110⟩, ⟨221⟩ zone axes (Figure 1 b–d) and corresponding high-resolution transmission electron microscopy (HRTEM) images (Figure 1 e–g). The tetragonal structure with space group *P*4/*mmm* for SNCF is consistent with the results reported by S. Van Rompaey et al.[13] The XRD pattern of ball-milled SNCF (SNCF-BM) is shown in the Supporting Information, Figure S1. The broadened diffraction peaks of lower comparable intensity displayed by the SNCF-BM material indicate the reduced grain size after ball milling.

The electrocatalytic activity of SNCF perovskite for the OER was evaluated by linear sweeping voltammograms (LSVs) in O_2-saturated 0.1 M KOH at a scan rate of $5\ mV\,s^{-1}$ and rotation speed of 1600 rpm. Similar measurements were performed on the SCF, BSCF, and IrO_2 catalysts for comparison. The potential is referenced to the reversible hydrogen electrode (RHE), which was calibrated as described in the Experimental Section (Supporting Information, Figure S2). All potential values are *iR*-corrected during each LSV to compensate for the resistance of the solution. In Figure 2 a, the LSVs of SNCF showed an OER onset potential (1.53 V) that is similar to SCF and BSCF, and slightly higher than the IrO_2 catalyst (1.47 V). However, ball-milled SNCF (SNCF-BM) exhibited a comparably low onset potential (1.49 V) and a greater catalytic current than the IrO_2 catalyst. Notably, conductive carbon showed negligible OER activity in the potential range studied. It is important to compare the relative values of the overpotential η required to achieve a current density of $10\ mA\,cm^{-2}$, which is a metric relevant to solar fuel synthesis.[14] Remarkably, the SNCF-BM catalyst afforded such current density at a comparably small η value (ca. 0.42 V), which is more negative than that of SNCF ($\eta =$ 0.50 V), SCF ($\eta = 0.53$ V), BSCF ($\eta = 0.51$ V), and IrO_2 ($\eta =$ 0.45 V). The SNCF electrocatalyst also showed higher activity than some currently reported high-performance OER catalysts (Supporting Information, Figure S3), such as double-perovskite $PrBaCo_2O_{5-\delta}$ (PBC),[11b] spinel-like $LiCoO_2$,[15] and the rhombohedral perovskite $LaNiO_{3-\delta}$ (LN).[11c,16] Each crystal structure was identified by their respective XRD patterns (Supporting Information, Figure S4).

To gain more information on the kinetics of OER, the Tafel plots of SNCF, BSCF, and IrO_2 catalysts were drawn in Figure 2 b. The Tafel slopes are 76, 94, and $83\ mV\,dec^{-1}$ (millivolt per decade of electrical current density) for SNCF, BSCF, and IrO_2, respectively. The SNCF catalyst exhibits the

smallest Tafel slope among the studied materials. Furthermore, the specific activity ($mA\,cm^{-2}{}_{ox}$) normalized to real oxide surface area, as estimated from BET measurements (Supporting Information, Figure S5), were also plotted as a function of potential (Figure 2c, inset). To our knowledge, the specific activity (SA) reflects the intrinsic activity of a catalyst for OER. From Figure 2c, at $\eta = 0.5$ V (η that needed to afford a current density of 10 $mA\,cm^{-2}$ for SNCF), we found that SNCF catalyzes the OER with an intrinsic activity at least an order of magnitude higher than the IrO_2 catalyst and is about twice that of BSCF, respectively. However, SNCF-BM displayed a higher Tafel slope (90 $mV\,dec^{-1}$) and lower specific activity than SNCF (Figure 2b,c). These results suggested that the intrinsic activity was deteriorated significantly by the ball milling process like that reported for BSCF by Shao-Horn et al.[11a] Unfortunately, the cause of this phenomenon is still unknown, but it is a worthy topic of future research.

In general, perovskite catalysts typically display low surface areas ($< 2\,m^2\,g^{-1}$) owing to their high calcination temperatures ($> 800\,°C$), which always results in low mass activity for both the oxygen reduction reaction (ORR) and the OER.[11a,17] Thus, reducing particle size is an efficient way to improve the mass activity of perovskite electrocatalysts.[11d,16,18] To reach this goal, ball milling is an easy and effective strategy to make particles in the submicrometer range (Supporting Information, Figure S6).[11a,19] The mass activity of the SNCF, BSCF, IrO_2, and SNCF-BM catalysts at $\eta = 0.5$ V is shown in Figure 2d. The mass activity of SNCF-BM is 93.15 $A\,g^{-1}$, which is about 2.5 and about 1.5 times higher than that of the BSCF and IrO_2, respectively. As expected, SNCF showed lower mass activity than SNCF-BM owing to its comparatively fewer OER active sites. Although the ball-milling process increased the specific surface area to some extent, it did not result in sufficient miniaturization of the SNCF particles. Therefore, nanostructured perovskites could be more promising alternative electrocatalysts in terms of further improvements to mass activity. According to the comparison of the OER activities, for example, $\eta =$ 10 $mA\,cm^{-2}$, Tafel slopes, specific activity, and mass activity (Supporting Information, Table S1), the SNCF catalyst is attested to possess the best intrinsic OER activity and its mass activity could be further enhanced through ball milling.

Long-term stability is another critical parameter that determines the practicability of electrocatalysts. To assess this, we performed continuous potential cycling between 1.147 and 1.947 V (versus RHE) for SNCF and SNCF-BM, with SCF, BSCF, and IrO_2 as reference, in O_2-saturated 0.1 M KOH. As shown in Figure 3a–d, after 1000 cycles, the OER current at 1.947 V (versus RHE) for SNCF slightly decreased by 7.9%, while much higher degradation rates of 15.6, 14.4, and 21.6% were observed for SCF, BSCF, and IrO_2, respectively. The good durability of the SNCF perovskite could be explained by the incorporation of high-valence Nb^{5+} cations on the B-site, serving to effectively enhance phase stability.[20] In contrast, SCF and BSCF was unstable because of a change of the local structure from corner-sharing to edge-sharing octahedral that accompanied leaching of $Ba^{2+}$and Sr^{2+} during cycling in alkaline solution.[12] IrO_2 displayed a sharp loss in OER

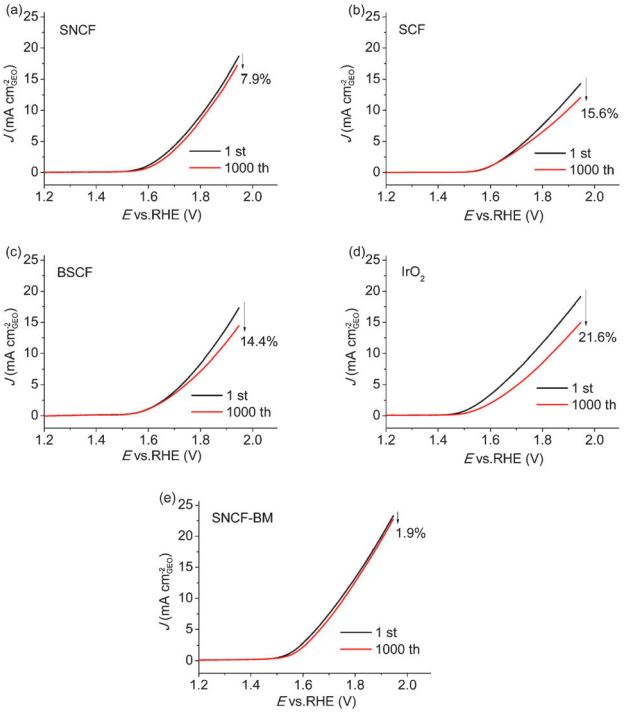

Figure 3. OER linear sweep voltammograms (LSVs) on rotating disk electrodes for the a) SNCF, b) SCF, c) BSCF, d) IrO_2 and e) SNCF-BM catalysts before and after 1000 cycles of accelerated stability testing in O_2-saturated 0.1 M KOH solution at 1600 rpm.

activity owing to oxidation of the surface Ir^{4+} to the water-soluble IrO_4^{2-} anion, as has been widely reported.[21] Remarkably, the durability of SNCF could be further improved through ball milling. SNCF-BM exhibited the best durability, with almost no OER activity decay (Figure 3e). This may be ascribed to better mechanical adhesion between active material and the GC (glassy carbon) substrate for SNCF-BM owing to higher specific surface area, which reduces the possibility of mechanical spalling from the electrode. Combining the above merits, the SNCF perovskite featured also an excellent durability during long-term operation.

The strong durability and superior activity of the SNCF perovskite indicate that it may be viable as an efficient OER catalyst. Understanding the source of the excellent OER performance is critical for designing even better materials. This could be related to the following several factors. Firstly, the electronic configuration of Co, with an optimal e_g orbital filling ($t_{2g}{}^5e_g{}^{1.2}$), was present in SNCF. Figure 4a shows the Co $2p_{3/2}$ XPS spectra of SNCF, which deconvoluted well into four peaks characteristic of Co^{2+} and Co^{3+} and their shake-up satellites (denoted as "sat").[9b,22] The calculated Co^{3+}/Co^{2+} ratios based on the area intensity was about 3.8, indicating that the average Co valences of the SNCF is assigned to be about 2.8. The valence state of Co in SNCF was further confirmed, combining the oxygen non-stoichiometry (δ) by iodometric titration method (Supporting Information, Table S2) with the Fe valences by Mössbauer spectroscopy (Supporting Information, Figure S7 and Table S3). Therefore, the e_g occupancy of cobalt in the SNCF perovskite is estimated to be 1.2, assuming that the Co^{3+} ions are in intermediate spin

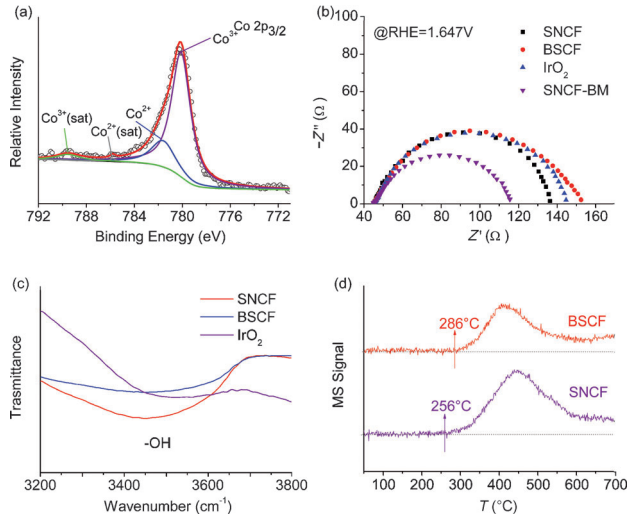

Figure 4. a) XPS spectra of Co $2p_{3/2}$ in the SNCF sample. b) Electrochemical impedance spectra of the SNCF, BSCF, IrO_2, and SNCF-BM electrodes recorded at 1.647 V versus RHE under the influence of an AC voltage of 10 mV. c) FTIR spectra of the SNCF, BSCF, and IrO_2 samples after exposure to water. d) O_2-TPD profiles of SNCF and BSCF samples.

states (IS) based on previous related studies.[23] However, it is noteworthy that the spin state estimation of Co^{3+} ion inferred from previous reports still gives rise to ambiguities owing to the difficulty in precisely distinguishing the multiple spin configurations. Therefore, further work is needed to confirm the Co^{3+} spin state in the SNCF perovskite. The e_g orbital filling ($t_{2g}^5e_g^{1.2}$) in SNCF is optimal for OER activity, which is the same as that in BSCF sitting on top of the volcano plot of activity versus e_g filling reported by Suntivich et al.[11a] Secondly, SNCF possessed good ionic and charge-transfer abilities between the electrolyte and the active material. Ion- and charge transport are crucial factors in the performance of efficient electrochemical OER catalysts. Charge transfer resistances were obtained by electrochemical impedance spectroscopy (EIS) measurements (Figure 4b). The charge-transfer resistance (R_{ct}) of SNCF (91.4 Ω) was smaller than that of BSCF (107.4 Ω) and IrO_2 (99.6 Ω). As a result, SNCF possessed a faster charge-transfer rate than the BSCF and IrO_2 catalysts during OER process.[24] SNCF-BM exhibited the lowest R_{ct} (70.6 Ω), indicating that the charge-transfer rate can be improved by increasing the active sites. Finally, the SNCF perovskite showed good OH^- adsorption and O_2 desorption capabilities. As observed by Fourier transform infrared (FTIR) spectroscopy (Figure 4c), a broad IR band with a maximum at approximately 3467 cm^{-1} appeared for the measured samples after exposure to water, corresponding to H-bonded OH stretching vibrations.[25] Obviously, SNCF exhibited a stronger OH absorption band than BSCF and IrO_2, indicating that SNCF possesses a stronger OH^- adsorption ability than either BSCF or IrO_2. Figure 4d showed the O_2 temperature-programmed desorption (O_2-TPD) profiles of SNCF and BSCF. The desorption peaks of SNCF occurred at nearly 256 °C, which is lower than BSCF (286 °C), indicating a greater O_2 desorption capability. These features resulted in the SNCF perovskite being an outstanding electrocatalyst for OER.

In summary, a novel tetragonal $SrNb_{0.1}Co_{0.7}Fe_{0.2}O_{3-\delta}$ (SNCF) perovskite was developed as an efficient OER catalyst with remarkable activity and stability in alkaline solutions. The SNCF perovskite exhibited a higher intrinsic OER activity and a smaller Tafel slope than the state-of-the-art precious-metal IrO_2 catalyst and the well-known BSCF perovskite. Several factors, including the presence of $Co^{2.8+}$ in SNCF with an optimal e_g orbital filling ($t_{2g}^5e_g^{1.2}$), good ionic and charge-transfer abilities,and high OH^- adsorption and O_2 desorption capabilities possibly contribute to the observed enhanced OER activity. To our knowledge, this material is the perovskite with the highest intrinsic OER activity yet reported. Moreover, SNCF also exhibited outstanding durability under harsh OER cycling conditions. Remarkably, the OER mass activity of SNCF by ball milling (SNCF-BM) was further improved, which was found to compare favorably comparable with the benchmark IrO_2. These merits speak to the potential of the SNCF perovskite as a promising OER catalyst for use in energy storage and conversion applications, such as solar water splitting, fuel cells, electrolysis, and metal–air batteries.

Keywords: intrinsic activity · energy storage and conversion · oxygen evolution reaction · perovskites

How to cite: *Angew. Chem. Int. Ed.* **2015**, *54*, 3897–3901
Angew. Chem. **2015**, *127*, 3969–3973

[1] a) S. Chu, A. Majumdar, *Nature* **2012**, *488*, 294; b) M. T. M. Koper, *Nat. Chem.* **2013**, *5*, 255; c) T. P. Cook, D. K. Dogutan, S. Y. Reece, Y. Surendranath, T. S. Teets, D. G. Nocera, *Chem. Rev.* **2010**, *110*, 6474.
[2] a) M. G. Walter, E. L. Warren, J. R. McKone, S. W. Boettcher, Q. Mi, E. A. Santori, N. S. Lewis, *Chem. Rev.* **2010**, *110*, 6446; b) J. A. Turner, *Science* **2004**, *305*, 972; c) H. B. Gray, *Nat. Chem.* **2009**, *1*, 7; d) M. Armand, J. M. Tarascon, *Nature* **2008**, *451*, 652; e) R. F. Service, *Science* **2009**, *324*, 1257.
[3] a) M. W. Kanan, D. G. Nocera, *Science* **2008**, *321*, 1072; b) H. Dau, C. Limberg, T. Reier, M. Risch, S. Roggan, P. Strasser, *ChemCatChem* **2010**, *2*, 724.
[4] a) Y. Lee, J. Suntivich, K. J. May, E. E. Perry, Y. Shao-Horn, *J. Phys. Chem. Lett.* **2012**, *3*, 399; b) F. A. Frame, T. K. Townsend, R. L. Chamousis, E. M. Sabio, T. Dittrich, N. D. Browning, F. E. Osterloh, *J. Am. Chem. Soc.* **2011**, *133*, 7264; c) C. C. L. McCrory, S. Jung, J. C. Peters, T. F. Jaramillo, *J. Am. Chem. Soc.* **2013**, *135*, 16977.
[5] a) N. H. Chou, P. N. Ross, A. T. Bell, T. D. Tilley, *ChemSusChem* **2011**, *4*, 1566; b) L. Trotochaud, J. K. Ranney, K. N. Williams, S. W. Boettcher, *J. Am. Chem. Soc.* **2012**, *134*, 17253; c) Y. G. Li, P. Hasin, Y. Y. Wu, *Adv. Mater.* **2010**, *22*, 1926; d) J. Landon, E. Demeter, N. Inoglu, C. Keturakis, I. E. Wachs, R. Vasic, A. I. Frenkel, J. R. Kitchin, *ACS Catal.* **2012**, *2*, 1793.
[6] a) M. R. Gao, Y. F. Xu, J. Jiang, S. H. Yu, *Chem. Soc. Rev.* **2013**, *42*, 2986; b) M. R. Gao, Y. F. Xu, J. Jiang, Y. R. Zheng, S. H. Yu, *J. Am. Chem. Soc.* **2012**, *134*, 2930.
[7] S. Cobo, J. Heidkamp, P. A. Jacques, J. Fize, V. Fourmond, L. Guetaz, B. Jousselme, V. Ivanova, H. Dau, S. Palacin, M. Fontecave, V. Artero, *Nat. Mater.* **2012**, *11*, 802.
[8] a) V. Artero, M. Chavarot-Kerlidou, M. Fontecave, *Angew. Chem. Int. Ed.* **2011**, *50*, 7238; *Angew. Chem.* **2011**, *123*, 7376; b) Q. S. Yin, J. M. Tan, C. Besson, Y. V. Geletii, D. G. Musaev,

A. E. Kuznetsov, Z. Luo, K. I. Hardcastle, C. L. Hill, *Science* **2010**, *328*, 342.

[9] a) Y. Y. Liang, Y. G. Li, H. L. Wang, J. G. Zhou, J. Wang, T. Regier, H. J. Dai, *Nat. Mater.* **2011**, *10*, 780; b) S. Chen, J. J. Duan, M. Jaroniec, S. Z. Qiao, *Angew. Chem. Int. Ed.* **2013**, *52*, 13567; *Angew. Chem.* **2013**, *125*, 13812.

[10] a) Z. P. Shao, S. M. Haile, *Nature* **2004**, *431*, 170; b) Y. L. Zhu, J. Sunarso, W. Zhou, S. S. Jiang, Z. P. Shao, *J. Mater. Chem. A* **2014**, *2*, 15454; c) T. Hibino, A. Hashimoto, T. Inoue, J. Tokuno, S, Yoshida, M. Sano, *Science* **2000**, *288*, 2031; d) Y. L. Zhu, Z. G. Chen, W. Zhou, S. S. Jiang, J. Zhou, Z. P. Shao, *ChemSusChem* **2013**, *6*, 2249.

[11] a) J. Suntivich, K. J. May, H. A. Gasteiger, J. B. Goodenough, Y. Shao-Horn, *Science* **2011**, *334*, 1383; b) A. Grimaud, K. J. May, C. E. Carlton, Y. L. Lee, M. Risch, W. T. Hong, J. G. Zhou, Y. Shao-Horn, *Nat. Commun.* **2013**, *4*, 2439; c) W. Zhou, J. Sunarso, *J. Phys. Chem. Lett.* **2013**, *4*, 2982; d) Y. L. Zhao, L. Xu, L. Q. Mai, C. H. Han, Q. Y. An, X. Xu, X. Liu, Q. J. Zhang, *Proc. Natl. Acad. Sci. USA* **2012**, *109*, 19569.

[12] a) M. Risch, A. Grimaud, K. J. May, K. A. Stoerzinger, T. J. Chen, A. N. Mansour, Y. Shao-Horn, *J. Phys. Chem. C* **2013**, *117*, 8628; b) K. J. May, C. E. Carlton, K. A. Stoerzinger, M. Risch, J. Suntivich, Y. L. Lee, A. Grimaud, Y. Shao-Horn, *J. Phys. Chem. Lett.* **2012**, *134*, 16959.

[13] S. Van Rompaey, W. Dachraoui, S. Turner, O. Y. Podyacheva, H. Tan, J. Verbeeck, A. Abakumov, J. Hadermann, *Z. Kristallogr.* **2013**, *228*, 28.

[14] Y. Matsumoto, E. Sato, *Mater. Chem. Phys.* **1986**, *14*, 397.

[15] a) S. W. Lee, C. Carlton, M. Risch, Y. Surendranath, S. Chen, S. Furutsuki, A. Yamada, D. G. Nocera, Y. Shao-Horn, *J. Am. Chem. Soc.* **2012**, *134*, 16959; b) T. Maiyalagan, K. A. Jarvis, S. Therese, P. J. Ferreira, A. Manthiram, *Nat. Commun.* **2014**, *5*, 3949.

[16] W. G. Hardin, D. A. Slanac, X. Q. Wang, S. Dai, K. P. Johnston, K. J. Stevenson, *J. Phys. Chem. Lett.* **2013**, *2*, 1254.

[17] J. Suntivich, H. A. Gasteiger, N. Yabuuchi, Y. Shao-Horn, *J. Electrochem. Soc.* **2010**, *157*, B1263.

[18] W. G. Hardin, J. T. Mefford, D. A. Slanac, B. B. Patel, X. Q. Wang, S. Dai, X. Zhao, R. S. Ruoff, K. P. Johnston, K. J. Stevenson, *Chem. Mater.* **2014**, *26*, 3368.

[19] J. Sunarso, A. A. J. Torriero, W. Zhou, P. C. Howlett, M. Forsyth, *J. Phys. Chem. C* **2012**, *116*, 5827.

[20] a) Y. L. Zhu, Y. Lin, X. Shen, J. Sunarso, W. Zhou, S. S. Jiang, D. Su, F. L. Chen, Z. P. Shao, *RSC Adv.* **2014**, *4*, 40865; b) K. Zhang, R. Ran, L. Ge, Z. P. Shao, W. Q. Jin, N. P. Xu, *J. Membr. Sci.* **2008**, *323*, 436; c) T. Nagai, W. Ito, T. Sakon, *Solid State Ionics* **2007**, *177*, 3433.

[21] a) A. Minguzzi, F. R. F. Fan, A. Vertova, S. Rondinini, A. J. Bard, *Chem. Sci.* **2012**, *3*, 217; b) E. Guerrini, H. Chen, S. Trasatti, *J. Solid State Electrochem.* **2007**, *11*, 939; c) P. Rasiyah, A. C. C. Tseung, *J. Electrochem. Soc.* **1984**, *131*, 803.

[22] a) T. Y. Ma, Y. Zheng, S. Dai, M. Jaroniec, S. Z. Qiao, *J. Mater. Chem. A* **2014**, *2*, 8676; b) Y. Xiao, C. G. Hu, L. T. Qu, C. W. Hu, M. H. Cao, *Chem. Eur. J.* **2013**, *19*, 14271.

[23] a) X. Wu, K. Scott, *J. Mater. Chem.* **2011**, *21*, 12344; b) I. O. Troyanchuk, D. V. Karpinsky, R. Szymczak, *Phys. Status Solidi B* **2005**, *242*, R49.

[24] T. Wang, L. Liu, Z. Zhu, P. Papakonstantinou, J. Hu, H. Liu, M. Li, *Energy Environ. Sci.* **2013**, *6*, 625.

[25] X. X. Zou, J. Su, R. Silva, A. Goswami, B. R. Sathe, T. Asefa, *Chem. Commun.* **2013**, *49*, 7522.

Received: September 11, 2014
Revised: December 20, 2014
Published online: February 4, 2015

